Order by disorder decision making via Berry flux

Benjamin O. Sung[1] and Michael J. Lawler[2,1]
[1]*Department of Physics, Cornell University, Ithaca, New York 14853, USA*
[2]*Department of Physics, Applied Physics and Astronomy, Binghamton University, Vestal, New York 13850, USA*
(Received 3 June 2016; revised manuscript received 18 August 2016; published 25 October 2016)

Order by disorder is a decision making process for frustrated systems but often leads to simple answers. We study order by disorder in the kagome Kondo model known for its complexity seeking rich decision making capabilities. At half-filling and large Kondo coupling to hopping ratio J_K/t, the full manifold of 120° kagome ground states are degenerate at second order in t/J_K. We show this degeneracy lifts at sixth order when a fermion can hop around a hexagon and feel the Berry flux induced by a given spin texture. Using the Monte Carlo method, we then seek the ground state of this sixth-order Hamiltonian and find in a 4×4 unit cell system that a coplanar 12-site unit cell order is selected over the $\sqrt{3}\times\sqrt{3}$,$q=0$ and cuboc1 states, a result that survives even in the thermodynamic limit. This state is selected for its SU(2) flux properties induced by the spin texture. Given the existence of numerous quantum Hall plateaus for electrons in a magnetic field, the existence of this 12-site unit cell state suggests that complex decision making is possible on the manifold of 120° states and achievable in different kagome Kondo models.

DOI: 10.1103/PhysRevB.94.144438

I. INTRODUCTION

Order by disorder [1] is a decision making process: different ground states will be selected from the same degenerate manifold depending on the type of fluctuations it experiences. The ground state with the highest entropy, for example, is selected when the thermal order by disorder effect is active. The ground state with the least zero-point energy, on the other hand, is selected when the quantum order by disorder effect is active. These examples are pedagogically discussed in a recent review [2]. In effect, the system computes the ground state according to the active order by disorder mechanism. In this way, the order by disorder effect fits into the subject of complexity science [3].

Yet, in most cases, order by disorder, either thermal, quantum, or another mechanism, selects a simple ground state. Naturally, this is expected in the simplest cases such as the J1-J2 model on the square lattice [4,5]. But for kagome antiferromagnets the coplanar $\sqrt{3}\times\sqrt{3}$ state is often [6] selected (or preferred if long-range order can not be established) both by thermal fluctuations [7] and quantum fluctuations [8,9]. This state has a tripled unit cell but is among the simplest in the massively degenerate kagome ground-state manifold. Even quantum order by disorder in pyrochlore Heisenberg antiferromagnets selects a colinear state [10] (though which colinear state is not clear at present [11]). Again, this is simpler than a general state in the massively degenerate manifold would suggest. So order by disorder seems to act as a de-complexifying mechanism.

In this light, the discovery of order by disorder in classical Kondo lattice models on highly frustrated lattices [12] is interesting. Complex orders, some of which have multiple wave vectors, are noncoplanar and are incommensurate, arise in these models on the square lattice [13], cubic lattice [14], triangular lattice [15], between the triangular and kagome lattices [16], and kagome lattice [12,17,18]. Further, the order by disorder effect on the kagome lattice model does not select either the $\sqrt{3}\times\sqrt{3}$ order or $q=0$ but possibly [12] the cuboc1 noncoplanar 120^0 state [19]. So it seems possible that order by disorder due to the fermion hopping in these models may give rise to complex selection among a highly degenerate ground-state manifold and that it is not decomplexifying.

Given the potential for complex orders, order by disorder in classical Kondo models could also be interesting should it produce an integer quantum Hall effect. This is possible [20,21] and, indeed, has provided much of the motivation for the study of these models [22]. In 2D, an effect is particularly expected at finite temperature should the complex order have a nonzero scalar spin chirality [23,24]. So, if the finite spin chirality [19,25] cuboc1 state were the selected state in the kagome case, order by disorder may provide a mechanism for the stability of a state with an integer quantum Hall effect.

In this paper, we revisit the order by disorder problem in the kagome Kondo lattice model with classical spins at half-filling. This problem is characterized by a small parameter t/J_K, a gap to electronic excitations and an SU(2) flux variable $\mathbf{U}$ felt by the electrons as they hop around in a background classical spin texture. By carrying out a perturbative expansion in t/J_K to sixth order, we show that the selection of a 120° state is due to the flux felt by an electron as it hops around a hexagon. Using the Monte Carlo technique, we then show that the state selected in a 4×4 unit cell system cluster with periodic boundary conditions has a 12-site unit cell. This state turns out to be precisely in between a $\sqrt{3}\times\sqrt{3}$ state and $q=0$ state: it has a spin origami sheet [26,27] that is fully folded in one direction and perfectly flat in the other. We have verified that it beats the $\sqrt{3}\times\sqrt{3}$,$q=0$ and cuboc1 state in the thermodynamic limit. Further, its SU(2) flux properties are also special: yielding energetic benefits both for hopping around hexagons and on bow ties (pairs of triangles). Finally, we have computed the electronic band structure and verified the absence of an integer quantum Hall effect as expected due to the vanishing scalar spin chirality. We conclude with an outlook on how these results may generalize to enable selection of other complex ordering patterns within the kagome 120° states and thereby achieve complex decision making among this manifold of states.

II. KONDO MODEL AND VARIATIONAL RESULTS

We begin with the Kondo Hamiltonian given by

$$H = H_{\text{hop}} + H_{\text{kondo}} = -t \sum_{\langle ij \rangle} c^{\dagger}_{i\sigma} c_{j\sigma} - J_k \sum_i S_i \cdot s_i. \quad (1)$$

Here, the Kondo term in the above Hamiltonian gives the coupling between the on-site classical spin vector S_i with the local electron spin $s_i = c_i^{\dagger} \tau c_i$ with coupling constant J_k. The first term above describes the electron hopping along adjacent sites on the given lattice with amplitude t.

The problem of finding the ground state of this model is then that of obtaining the optimal set of classical S_i spin vectors with the energy of any given set of S_i vectors determined from the Hamiltonian of noninteracting electrons hopping in the presence of a local magnetic field $h_i = J_K S_i$.

The case of weak coupling $\frac{J_k}{t} \ll 1$ is well-known and it was discovered that incommensurate noncoplanar multiwave vector spin orderings dominate the phase diagram [12]. In particular, aside from some exceptions, the Fermi surface geometry dictated the complex orderings in this limit.

At the opposite end, it is well known that in the double exchange model, i.e., the limit $J_k \to \infty$, the ferromagnetic state dominates over all other spin states at all but half-filling. There, instead of ferromagnetism, a gap in the fermion spectra opens up and antiferromagnetism is found [12]. The leading antiferromagnetic term turns out to be just a nearest-neighbor Heisenberg model.

A quick exploration of the landscape of magnetism is easily achieved using a variational calculation that takes into account just the collinear ferromagnetic and coplanar antiferromagnetic $q = 0$ states. By exact diagonalizing the above Hamiltonian on a finite 12×12 kagome lattice with imposed periodic boundary conditions, we obtain the phase diagram of Fig. 1, which qualitatively agrees with Ref. [12].

In Fig. 1, we have only portrayed the two simplest states of many well-known states on the Kagome lattice with a focus on the general competition between ferromagnetism and antiferromagnetism. The figure suggests that for $\frac{J_k}{t} \gg 1$, all states tend to converge to the same energy at half-filling in the double exchange model. However, one can slightly weaken this condition, and only consider the approximation $\frac{J_k}{t} \gg 1$ and consider which states dominate in this regime. To second order in perturbation theory in $\frac{J_k}{t}$, all 120° degree states are degenerate [12].

In addition to $q = 0$ and $\sqrt{3}\times\sqrt{3}$ states, there are an infinite number of other 120° spin configurations, both coplanar and noncoplanar, that one may place on an arbitrarily large, finite kagome lattice, and to second order in perturbation theory are all degenerate in energy. In order to extract a true, unique ground state out of the degenerate 120° spin state manifold, we must proceed to higher orders in perturbation theory.

In this paper, we will show that the degeneracy is lifted exactly at sixth order and exhibit a newly found state with a 12-site unit cell via a Monte Carlo simulation that beats the above well-known 120° states. Here, we can begin to understand this result with numerical evidence that the degeneracy is lifted at sixth order.

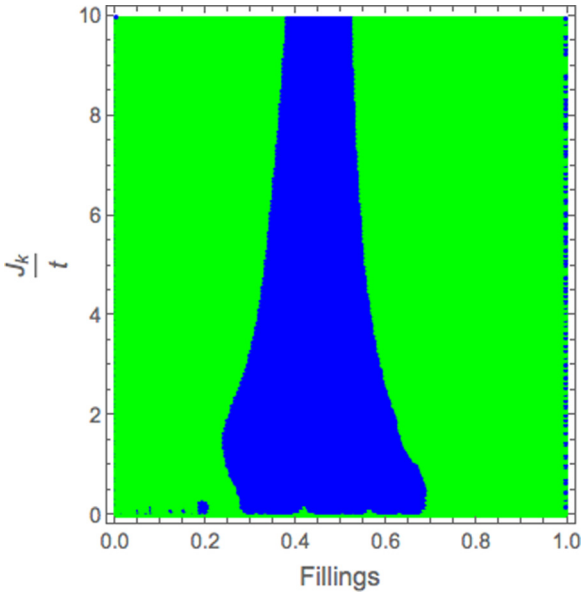

FIG. 1. Simplified variational phase diagram of kagome Kondo model with classical spins. Green: ferromagnetic, blue: $q = 0$. Over 432 sites where there are 12 triangles along the x axis and 12 triangles along the y axis. The horizontal axis represents the fraction of electrons occupying a site. The vertical axis is the ratio $\frac{J_k}{t}$.

Our numerical argument follows by presenting the energy data for three well-known 120° states. The energy data for these spin configurations were obtained by exact diagonalizing the Hamiltonian given in equation (1) and summing the lower half of the eigenvalue spectrum, corresponding to half-filling. On a 24×24 kagome lattice, the first few energy values in terms of the coupling constant J_k are as in the table below.

J_k	q = 0	$q = \sqrt{3}\times\sqrt{3}$	cuboc1
1	−3388.466	−3409.835	−3387.137
2	−4530.299	−4535.492	−4535.302
3	−5967.679	−5968.139	−5968.586
4	−7522.879	−7522.914	−7523.120
5	−9138.454	−9138.446	−9138.537

We easily see that at small J_k, the energy data for the three 120° states differ slightly, due to nontrivial subleading terms in higher-order perturbation theory. However, as we increase J_k, terms of order n in perturbation theory are suppressed by the factor $\frac{1}{J_k^{n-1}}$, and hence the energies begin to converge. By $J_k/t = 3$, the cuboc1 state is dominating, closely followed by the $q = \sqrt{3}\times\sqrt{3}$ state and then the $q = 0$ state. By $J_k/t = 5$, the rankings of the states by energies are shifted, and we have the ranking of states cuboc1 $< q = 0 < \sqrt{3}\times\sqrt{3}$ which persists in the limit $J_k/t \to \infty$.

We now extend this numerical evidence for degeneracy splitting among the 120° states at sixth order. By acquiring energy data as in the above for the spectrum $J_k = 1$ to 100, and taking the differences in energies, we obtain Fig. 2 and clear evidence that the degeneracy is lifted at sixth order.

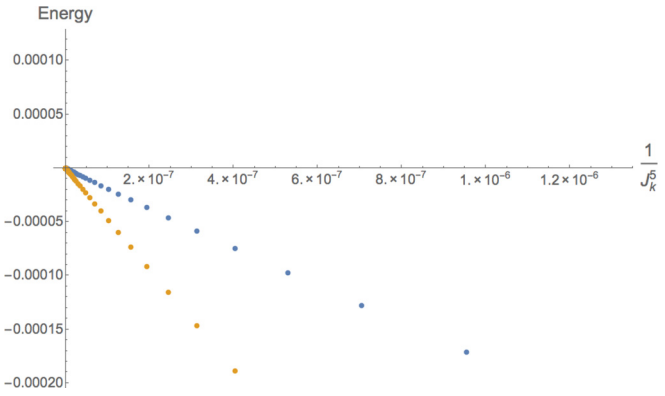

FIG. 2. Graph of J_k vs Energy. The energy values from $J_k = 1$ to 100 are plotted. The blue dots correspond to the difference between the states $q = 0$ and $q = \sqrt{3}\times\sqrt{3}$ and the yellow dots correspond to the difference between the states cuboc1 and $q = \sqrt{3}\times\sqrt{3}$ states. The fx axis is $\frac{1}{J_k^5}$ as J_k goes from 1 to 100, and the y axis are the energy values. The linearity of the two plots shows that the degeneracy breaks first at sixth order in perturbation theory. Energy calculations were run on a 24×24 kagome lattice.

Having shown numerically that degeneracy breaks at sixth order, one may calculate the contributions from each order in perturbation theory via numerical fitting. Specifically, by carrying out an asymptotic fitting of the energy data we obtain the results in the following table. However, due to noise, the accuracy drops with increasing order. We find order 2 is accurate to ±1, order 3 accurate to ±50, and order 5 accurate to ±250 (since orders 3 and 5 should be zero in the table).

Order of $\frac{1}{J_k}$	Numerical coefficients
2	−2591.73
3	45.4979
4	2751.6
5	−233.15

Looking at these results in isolation, the fifth-order term extracted this way suggests a probable nontrivial coefficient. So these numerical data would not be sufficient to determine the exact formula for any contributions from higher orders in perturbation theory. However, it does provide us with a check on our analytic calculation below.

III. FEYNMAN DIAGRAM APPROACH

A. Road map of Feynman diagram calculation

Here, we provide a road map for our Feynman diagram calculation. We proceed through the canonical method, writing down the path integral Z using our free Hamiltonian (1) without the hopping term. As usual, completing the square yields the propagator for the free theory. Adding the interaction (hopping term) and taking functional derivatives yields the full propagator for our theory. By taylor expanding in the perturbation H_{hop}, we obtain the interaction U_{ij}, which may be readily computed via unitary diagonalization as a 2×2 matrix describing the hopping between nearest neighbor sites. We then calculate the energy corrections via the formula (8), which was calculated using the linked cluster theorem. We further highlight the procedure for the first two orders in perturbation theory and show that they agree with results from the usual quantum mechanical procedure.

B. Derivation of Feynman rules

We first determine the Feynman rules for our interaction vertex. To do this, note that we must calculate the amplitude for hopping between two sites given by some unitary 2×2 matrix U_{ij}, corresponding to up and down spin states. We begin with Eq. (1) in the matrix representation

$$H = \begin{pmatrix} -J_k S^z & -J_k S^x - i J_k S^y \\ -J_k S^x + i J_k S^y & J_k S^z \end{pmatrix}. \tag{2}$$

Diagonalizing is then just choosing a basis where S_i points in the z direction. We obtain the unitary matrices

$$U = \begin{pmatrix} \frac{-S^x - iS^y}{\sqrt{2+2S^z}} & \frac{S^x + iS^y}{\sqrt{2-2S^z}} \\ \frac{S^z+1}{\sqrt{2+2S^z}} & \frac{-S^z+1}{\sqrt{2-2S^z}} \end{pmatrix}, \quad U^\dagger = \begin{pmatrix} \frac{-S^x + iS^y}{\sqrt{2+2S^z}} & \frac{S^z+1}{\sqrt{2+2S^z}} \\ \frac{S^x - iS^y}{\sqrt{2-2S^z}} & \frac{-S^z+1}{\sqrt{2-2S^z}} \end{pmatrix}. \tag{3}$$

Expressing the hopping H_{hop} in terms of unitary matrices, we obtain

$$H_1 = -t \sum_{\langle ij \rangle} (U^{i\dagger}_{\sigma\sigma'} U^j_{\sigma\sigma''}) c^\dagger_{i\sigma'} c_{j\sigma''} + \text{H.c.} \tag{4}$$

Finally, writing out the product of the unitary matrices explicitly, for hopping between two sites with classical spin vectors S_i and S_j, we obtain

$$\begin{aligned}
U_{11} &= \frac{1}{\sqrt{2+2S^{z^i}}\sqrt{2+2S^{z^j}}}(S^{x^i}S^{x^j} - iS^{y^i}S^{x^j} + iS^{x^i}S^{y^j} \\
&\quad + S^{y^i}S^{y^j} + S^{z^i}S^{z^j} + S^{z^i} + S^{z^j} + 1), \\
U_{12} &= \frac{1}{\sqrt{2+2S^{z^i}}\sqrt{2-2S^{z^j}}}(-S^{x^i}S^{x^j} + iS^{y^i}S^{x^j} - iS^{y^j}S^{x^i} \\
&\quad - S^{y^i}S^{y^j} - S^{z^i}S^{z^j} + S^{z^i} - S^{z^j} + 1), \\
U_{21} &= \frac{1}{\sqrt{2-2S^{z^i}}\sqrt{2+2S^{z^j}}}(-S^{x^i}S^{x^j} + iS^{y^i}S^{x^j} - iS^{x^i}S^{y^j} \\
&\quad - S^{y^i}S^{y^j} - S^{z^i}S^{z^j} + S^{z^j} - S^{z^i} + 1) \\
U_{22} &= \frac{1}{\sqrt{2-2S^{z^i}}\sqrt{2-2S^{z^j}}}(S^{x^i}S^{x^j} - iS^{y^i}S^{x^j} + iS^{x^i}S^{y^j} \\
&\quad + S^{y^i}S^{y^j} + S^{z^i}S^{z^j} - S^{z^i} - S^{z^j} + 1).
\end{aligned} \tag{5}$$

We now derive the propagator Feynman rules for our theory using the path integral approach. Proceeding via Grassman variables, we take $H_{\text{kondo}} = -J_k \sum_{\langle ij \rangle} S_i \cdot s_i$ as the unpertrubed Hamiltonian with partition function

$$\begin{aligned}
Z &= \int Dc D\bar{c} \exp\left(i \int dt \left[\sum_i i\bar{c}_{i\sigma} \partial_t c_{i\sigma} - H \right] \right) \\
&= \int Dc D\bar{c} \exp\left(i \int dt \left[\sum_i i\bar{c}_{i\sigma} \partial_t c_{i\sigma} \right. \right. \\
&\quad \left. \left. + J_k \sum_i S_i \cdot \bar{c}_{i\sigma} \tau_{\sigma\sigma'} c_{i\sigma'} + \sum_i (\bar{\eta}_{i\sigma} c_{i\sigma} + \bar{c}_{i\sigma} \eta_{i\sigma}) \right) \right).
\end{aligned} \tag{6}$$

To calculate the propagator for our free theory, we Fourier transform to frequency space, complete the square, and transform to the z basis, which we fixed in the diagonalization above, obtaining the Green's function

$$G^{\sigma_1\sigma_2}_{j_1 j_2} = \frac{\delta_{j_1,j_2}\delta^{\sigma_1,\sigma_2}}{\omega - J_k\tau^3_{\sigma_1,\sigma_2} + i\epsilon sgn(\omega)}, \tag{7}$$

where the upper indices denote spin indices, and the lower indices denote points in position space.

C. Energy calculation

In full, the above calculation gives us the following Feynman rules:

$G^{\sigma\sigma'}_{ij}$

i,σ —— j,σ'

$U^{\sigma\sigma'}_{ij}$

i,σ ~~~~ j,σ'

To calculate an nth order process, the Taylor expansion tells us to connect n G's and n U's in an alternating order. Intuitively, one may think of the propagator as the virtual electron hopping between nearest neighbors, and the interaction U as imposing the constraint that the path traversed by the virtual electron must be connected.

Before moving to sixth order, we give a sample calculation to first and second order. We begin with first order, to check that our path integral does indeed give zero for only one hopping.

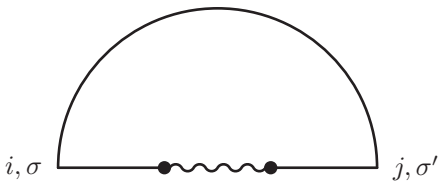

The expression to calculate the energy is given by

$$\begin{aligned} E &= -\frac{i}{T}\ln(Z_0) - \frac{i}{T}\ln\left(\left\langle\exp\left(-i\int dt H_I\right)\right\rangle\right) \\ &= E^{(0)}_G - \frac{i}{T}\ln\left(\left\langle\exp\left(-\frac{i}{T}\int dt H_I\right\rangle_0\right). \end{aligned} \tag{8}$$

Hence, proceeding with the calculation for first-order processes, we obtain

$$\begin{aligned} E' &= \int d\tau - t\sum_{ij}\langle\overline{c_{i\sigma}(t)}U^{\sigma\sigma'}_{ij}c_{j\sigma'}(t)\rangle \\ &= tTr\int_{t_1}^{t_2} d\tau\sum_{ij} G_{ij}(t-t)U_{ij} \\ &= tT\sum_{ij}\int\frac{d\omega}{2\pi}G_{ij}(\omega)U_{ij.} \end{aligned} \tag{9}$$

Now, noting that the Green's function gives the delta function $G_{ij} \propto \delta_{ij}$ and that U_{ij} vanishes identically for $i = j$, we see that the correction vanishes.

We now consider the integral to second order. In this case, we have the diagram

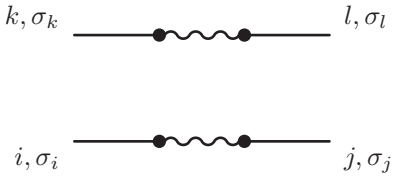

Here, we have two horizontal lines corresponding to two vertices on the kagome lattice. Although not indicated, we choose the convention with the direction of propagation to the right, hence, we may only connect, using a propagator, a vertex at the left with a vertex at the right. For instance, we may connect (k,σ_k) with (j,σ_j), but not (k,σ_k) with (i,σ_i). Note that there are only two distinct ways to connect using propagators as indicated below.

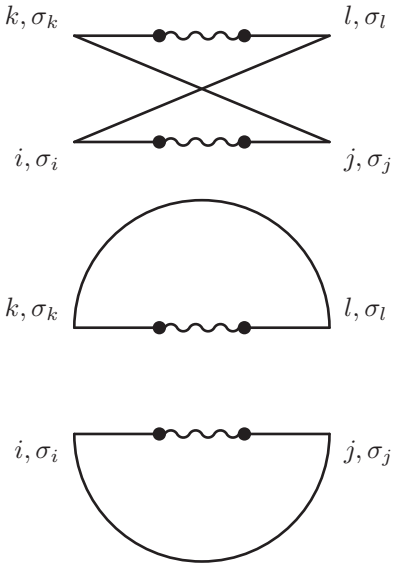

As shown, the second diagram is disconnected, and hence it does not contribute to the energy correction at second order. Evaluating the first diagram as usual, one can verify that we obtain the correction

$$\begin{aligned} E' &= \mathrm{Tr}\left(\int\frac{d\omega}{2\pi}\sum_{ijkl} G_{li}U_{ij}G_{jk}U_{kl}\right) \\ &= -\frac{3}{8}J_k^2, \end{aligned} \tag{10}$$

where the spin indices have been suppressed where the second line has been evaluated for the case of 120° states. This answer agrees with our calculation using the unitary matrices and the usual quantum mechanical perturbative energy formula.

We may carry this procedure out to sixth order, with which we will obtain the expression

$$E'^6 = \mathrm{Tr}\left(\int\frac{d\omega}{2\pi}\sum GUGUGUGUGUGU\right), \tag{11}$$

where spatial and and spin indices have been suppressed. We remark that there is no need to connect all the possible lines in a single six-order Feynman diagram since the energy sums over all possible spatial indices. Hence, with these Feynman

rules, we may derive perturbative energy corrections to any order with a single Feynman diagram.

Remarkably, we can interpret each term in the sum over six site plaquettes that contribute to E'^6 as an SU(2) flux. The SU(2) gauge field here is classical and we can identify it in the Hamiltonian if we place it in the form

$$H = \sum_{\langle ij \rangle} c_i^\dagger U_{ij} c_j + \text{H.c.} - \sum_i c_i^\dagger \mathbf{A}_{0i}(t) c_i, \tag{12}$$

where in the basis of Eq. (1) we have $\mathbf{A}_{0i} = J_K S_i \cdot \tau$ [see Eq. (2)] and $U_{ij} = \tau_0$, while after the basis transformation that follows Eq. (2), we have $\mathbf{A}_{0i} = J_K \tau_3$ and $U_{ij} = U^{i\dagger} U^j$ given by Eq. (5). Thus the change of basis can be viewed as an SU(2) gauge transformation. Additionally, the propagators G_{ij} transform under a gauge transformation as $G_{ij}(t) \to G_{ij}(t) e^{i(\theta_i(0) - \theta_j(t))}$ and so are proportional to the time-component of the Wilson line of the SU(2) gauge field

$$G_{ij}(t) \propto \delta_{ij} T e^{i \int_0^t dt' A_{0i}(t)}. \tag{13}$$

One can determine the proportionality constant [28] but we do not need it here. Thus, after inverse Fourier transforming Eq. (11) from frequency space to real time, we see it is a time average over Wilson loops that enclose the hexagon but additionally propagate along the time direction. An example is shown in Fig. 3. Thus the degeneracy in the large J_k/t expansion is lifted by the time average of the SU(2) flux penetrating time-dependent Wilson loops.

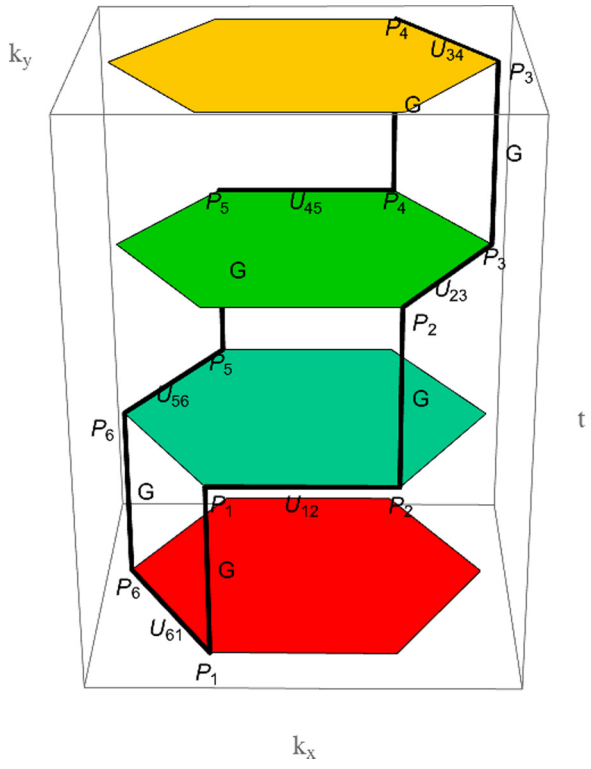

FIG. 3. Plot of example loop given by Eq. (11). The paths indicated by U_{ij} represent virtual hoppings in momentum space, while the paths given by the Green's function G, represent virtual hoppings forward or backward in time. The nontrivial flux is given by the combination of electric and magnetic flux; it is easy to see that taking only the magnetic flux gives a trivial result.

IV. NUMERICAL CALCULATIONS

A. Analytical preliminaries

Clearly, it is necessary to numerically evaluate the analytical expression obtained from Feynman diagrammatic techniques for energy corrections of order $n > 2$. To do this, we separate Eq. (11) into a linear combination of Pauli matrices as shown below.

We define the variables

$$\mu = \frac{1}{2}\left(\frac{1}{\omega - J_k + i\epsilon} + \frac{1}{\omega + J_k - i\epsilon}\right),$$
$$\nu = \frac{1}{2}\left(\frac{1}{\omega - J_k + i\epsilon} - \frac{1}{\omega + J_k - i\epsilon}\right), \tag{14}$$

and

$$\begin{aligned}
\alpha = \frac{1}{2}\Bigg(&\frac{1}{\sqrt{2+2S_{x_3}}\sqrt{2+2S_{y_3}}}(S_x \cdot S_y - iS_{x_2}S_{y_1} \\
&+ iS_{x_1}S_{y_2} + S_{x_3} + S_{y_3} + 1) \\
&+ \frac{1}{\sqrt{2-2S_{x_3}}\sqrt{2-2S_{y_3}}}(S_x \cdot S_y - iS_{x_2}S_{y_1} \\
&+ iS_{x_1}S_{y_2} - S_{x_3} - S_{y_3} + 1)\Bigg), \\
\delta = \frac{1}{2}\Bigg(&\frac{1}{\sqrt{2+2S_{x_3}}\sqrt{2+2S_{y_3}}}(S_x \cdot S_y - iS_{x_2}S_{y_1} \\
&+ iS_{x_1}S_{y_2} + S_{x_3} + S_{y_3} + 1) \\
&- \frac{1}{\sqrt{2-2S_{x_3}}\sqrt{2-2S_{y_3}}}(S_x \cdot S_y - iS_{x_2}S_{y_1} \\
&+ iS_{x_1}S_{y_2} - S_{x_3} - S_{y_3} + 1)\Bigg), \\
\beta = \frac{1}{2}\Bigg(&\frac{1}{\sqrt{2+2S_{x_3}}\sqrt{2-2S_{y_3}}}(-S_x \cdot S_y + iS_{x_2}S_{y_1} \\
&- iS_{y_2}S_{x_1} + S_{x_3} - S_{y_3} + 1) \\
&+ \frac{1}{\sqrt{2-2S_{x_3}}\sqrt{2+2S_{y_3}}}(-S_x \cdot S_y + iS_{x_2}S_{y_1} \\
&- iS_{y_2}S_{x_1} - S_{x_3} + S_{y_3} + 1)\Bigg), \\
\gamma = \frac{1}{2}\Bigg(&\frac{1}{\sqrt{2+2S_{x_3}}\sqrt{2-2S_{y_3}}}(-S_x \cdot S_y + iS_{x_2}S_{y_1} \\
&- iS_{y_2}S_{x_1} + S_{x_3} - S_{y_3} + 1) \\
&- \frac{1}{\sqrt{2-2S_{x_3}}\sqrt{2+2S_{y_3}}}(-S_x \cdot S_y + iS_{x_2}S_{y_1} \\
&- iS_{y_2}S_{x_1} - S_{x_3} + S_{y_3} + 1)\Bigg),
\end{aligned} \tag{15}$$

and rewrite the Green's function and unitary matrices as

$$\frac{1}{\omega - J_k \tau^3_{\sigma 2 \sigma 2}} = \mu \tau^0 + \mu \tau^3$$
$$U^{\sigma\sigma'}_{ij} = \alpha \tau^0 + \beta \tau^1 + \delta \tau^2 + \gamma \tau^3. \quad (16)$$

Consequently, we may rewrite Eq. (11) by substituting in these linear combinations, and evaluate it numerically in MATHEMATICA. We find to third and fifth order that the energy correction vanishes as expected from the numerical results.

Intuitively, we may think of the numerical result that degeneracy is first lifted at sixth order as follows. Second order in perturbation theory selects out a degenerate manifold of 120° states. Since third and fifth order vanishes, the fourth-order term is the only possible nontrivial contribution. However, if we think of the electron as hopping around paths with the condition that it begins and ends on the same vertex, it is easy to see that there are no nontrivial loops that could be achieved via four hoppings. This is only viable at sixth order, in which the electron may hop across bow-tie loops and hexagon loops. In particular, we verify numerically using the above procedure that fourth order terms are identical for the well-known 120° states on the kagome lattice. We attribute the nontrivial sixth order contribution as resulting from the Berry's phase.

We further proceeded via a simulation on a 4×4 kagome lattice, on which we evaluated the above expression numerically and verified that the cuboc1 state dominates over the $q = 0$ state at sixth order as expected. Having derived this expression, this motivates us to carry out a Monte Carlo simulation to find a global minimum of this theory. In the next section, we detail the results that we obtained using a nonlinear local optimization method.

B. Numerical nonlinear local optimization

Using the expression derived above, we may numerically evaluate the sixth-order contributions from any spin configuration on the kagome lattice. To do this, we create an ensemble of 1000 random spin configurations on the 4×4 kagome lattice. We chose the system size of a 4×4 kagome lattice since we want a small size system to simplify calculations. In particular, this is the smallest size system without six-site loops due to periodic boundary conditions that do not occur in the infinite size limit. We then proceed to numerically minimize each random spin configuration by imposing the 120° condition, i.e., neighboring on-site spin vectors must have an inner product of $-\frac{1}{2}$ using the NMinimize method in MATHEMATICA. We then calculate the sixth-order contribution of each of these 120° states. Upon doing this, we encountered a new state, with energy lower than any other well-known state, which we will detail below.

By calculating the sixth-order flux contributions to E'^6 on each six site plaquette discussed previously, we can understand how different spin configurations compete for the ground state in the large J_k/t limit. This calculation is summarized graphically in Fig. 4, which portrays the relative contributions.

As shown, the sixth-order contribution from the "snake state" dominates over both the $q = 0$ and cuboc1 states. We

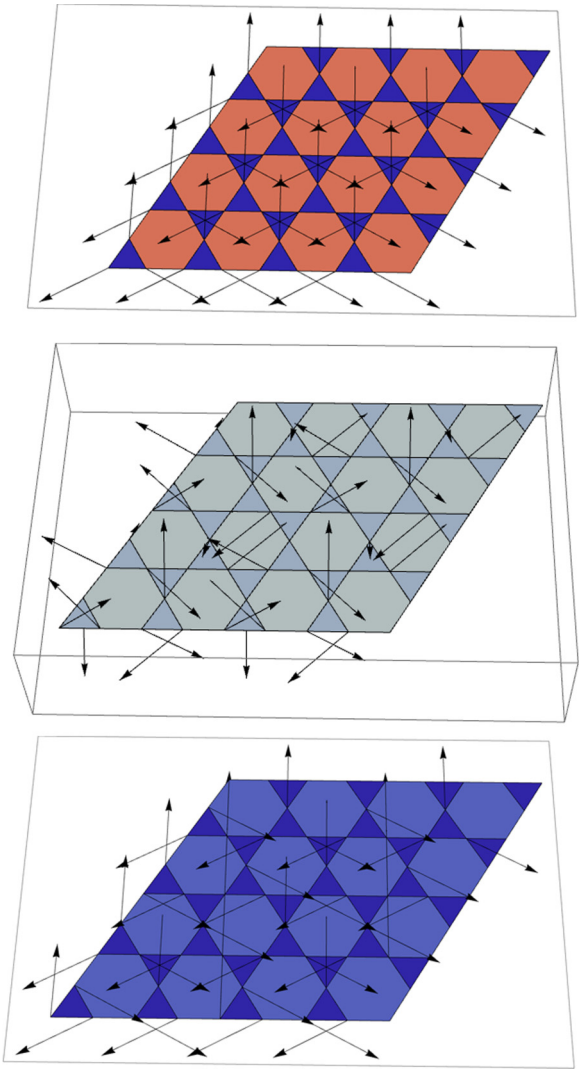

FIG. 4. Spin pattern plots that contribute at sixth order. For each bow-tie and hexagon loops, we compute using Eq. (11) where we take each U to correspond to an edge along the path between spin sites. Since there are two distinct bow-tie loops, we pick a canonical choice of traversing the bow-tie loop. We compare the relative values of these energy contributions from paths of length six using a temperature scale. The colors correspond to the values of the fluxes through the loops, i.e., "hotter" colors are greater and "colder" colors are smaller. Top figure is the $q = 0$ state, middle figure is the cuboc1 state, and the bottom figure is the "snake" state.

now proceed to discuss some properties of the newly found state.

To give a better visualization of our state, we will employ the technique of spin origami [26,27] as plotted in Fig. 5. For each hexagon in the kagome lattice, we may assign a "height vector" $h_i, i \in \{1, \ldots, N\}$, where N is the number of hexagons. Observe that every pair of adjacent hexagons corresponds uniquely to a spin vector, defined by a given spin configuration. To construct the spin origami sheet, let $h_0 = \{0,0\}$, corresponding to an arbitrary initial hexagon. We may then recursively obtain the next height vector $h_1 \equiv h_0 \pm S_{0,1}$ where $S_{0,1}$ is the unique spin vector lying between the two hexagons, and the sign is defined by the corresponding spin

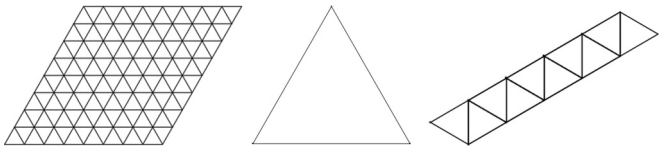

FIG. 5. Spin origami plots [26,27] that map a 120° state to a folded sheet of paper. Left state is the $q = 0$ pattern that maps to a flat sheet of paper. Middle is the $\sqrt{3}\times\sqrt{3}$ state that maps to a single triangle (completely folded sheet of paper). Right is the snake state that maps to a strip that is flat in one direction and completely folded in the other. Each of these patterns corresponds to an 8×8 kagome lattice with open boundary conditions. As indicated, the snake spin state exhibits a spin origami pattern that appears to lie between the $q = 0$ and $q = \sqrt{3}\times\sqrt{3}$ spin origami plots.

vector in a $q = 0$ reference state with spins lying in the plane of the lattice and pointing from the centers of one hexagon to another. For instance, if the corresponding spin vector in the $q = 0$ lattice was oriented from H_0 to H_1, where H_i, denotes the ith hexagon, then the corresponding height vector would be defined by $h_1 \equiv h_0 + S_{0,1}$, and a minus sign otherwise.

Figure 6 explains our name for this newly found state. The traversal of "ABABAB . . . " movements takes on a "snakelike" shape on the kagome lattice. Further evidence that the "snake" state is indeed the minimum of all our present states is given by Fig. 7 (cf. Fig. 2), which also exhibits the breaking of degeneracy of all three states at sixth order due to the linearity of the plots. As clearly shown on the same figure, the snake state indeed exhibits lower energies than the $q = 0$,$q = \sqrt{3}\times\sqrt{3}$, and cuboc1 states as calculated on the 24×24 kagome lattice. The reader should note that this verification is completely independent of our perturbation theory. This was calculated using only the Hamiltonian for the system and inputting the relevant data for the classical spin vectors for the snake state.

We now make one further remark regarding the spin plots displayed in Fig. 4. For coplanar 120° states on the kagome lattice, it can be shown that only hexagonal fluxes contribute to the breaking of degeneracies since the bow-tie loops all contribute the same energy. As detailed in the table below, the contributions of hexagonal fluxes are completely consistent

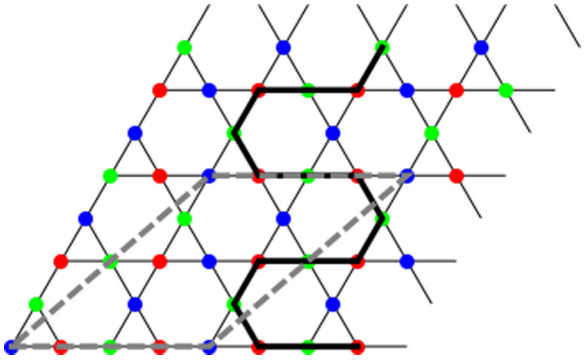

FIG. 6. The newly found state is called the snake state due to the above behavior of alternating colors traced out by the black path. It is a coplanar state with red, green, and blue colors corresponding to the usual spins on the $q = 0$ and $q = \sqrt{3}\times\sqrt{3}$ states. The unit cell is portrayed as the parallelogram bounded by the dashed gray lines.

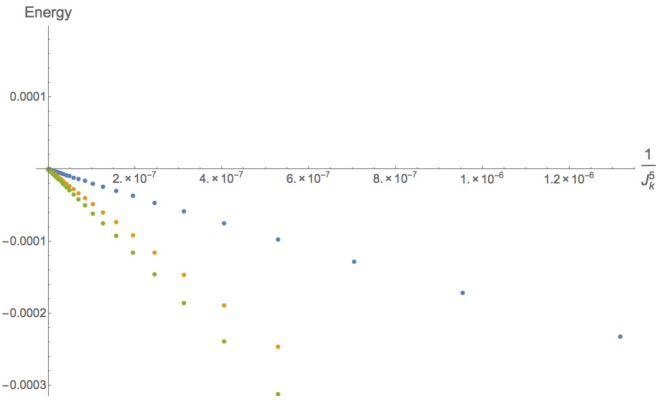

FIG. 7. The additional green line denotes the difference in energies for $J_k = 1$ to 100 between the snake and $q = \sqrt{3}\times\sqrt{3}$ states. This clearly shows that to sixth order, degeneracy among the 120° states is broken, and our snake state is the winner. Energy calculations were run on a 24×24 kagome lattice.

with our observations that at sixth order, we have the ordering of states: snake < cuboc1 < $q = 0$ < $q = \sqrt{3}\times\sqrt{3}$. Bow tie 1 was defined by traversing the bow-tie loop by crossing diagonally from the first triangle to the second, while bow tie 2 was defined by crossing from the first to the second triangle along the same side.

Classical State	Bow tie 1	Bow tie 2	Hexagon
$q = \sqrt{3}\times\sqrt{3}$	0.158203	−0.251953	0.333984
$q = 0$	0.158203	−0.251953	0.158203
Cuboc1	0.0214844	−0.115234	−0.0878906
Snake	0.158203	−0.251953	−0.193359

C. Chern number for the snake state

Finally, we have computed the electronic band structure of the snake state and its associated Chern number. The band structure for the filled bands is shown in Fig. 8. We have further computed the Chern number following Ref. [29]. We find both

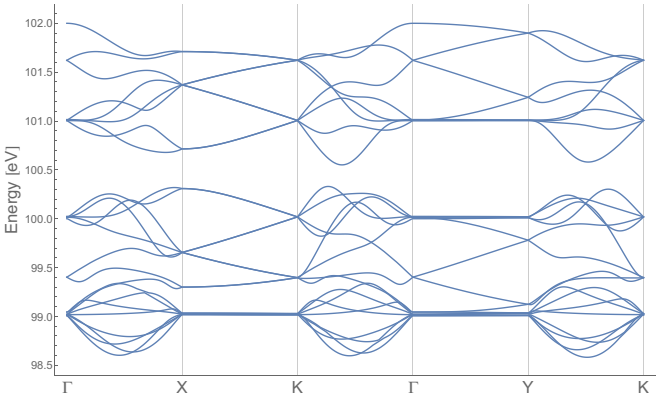

FIG. 8. Electronic band structure for the electrons hopping in the background of magnetic ordering of the snake state. Here the Brillouin zone is rectangular with sides at the X and Y points and corners at the K point.

for the bottom group of 16 bands and the next group of eight bands (together making the 24 filled bands out of 48 bands present in the snake state) have a vanishing Chern number. So order by disorder, at least as determined within our 4×4 unit cell calculation, is not selecting a state that could support an integer quantum Hall effect.

V. CONCLUSION

In this paper, we explored the problem of state selection at half-filling of the kagome Kondo model with classical spins. We were motivated to derive an analytical expression for higher orders in perturbation theory in order to better understand the degenerate 120° state manifold and achieved this to sixth order.

Proceeding via a numerical nonlinear local optimization algorithm, we find, out of an ensemble of 1000 random 120° states, a state that beats all the other well-known state as readily verified numerically via Fig. 7. In particular, combining the 120° state minimization along with the sixth order expression in the algorithm, we find that many of the runs readily converge to this state. Further work in this direction would include working with a larger ensemble with a more powerful machine in an attempt to find an even better ground state. In particular, we would like to fully understand the contribution of the fluxes to the sixth order correction. While we are drawn to the conclusion that the hexagon fluxes are responsible for the relative correction among the coplanar 120° states, we are not completely sure as to how the bow-tie and hexagon fluxes contribute to the noncoplanar 120° states.

It is remarkable that the snake state we find has a unit cell with 12 spins but was found in a calculation with 48 spins (4×4 unit cells). This suggests, another state with an even larger unit cell may ultimately win the order by disorder competition. However, even if this is not the case, order by disorder due to fermion hopping and associated Berry flux has selected a 120^0 state that to our knowledge has never been considered before. Hence complex ground states can arise from an order by disorder mechanism.

There is also the question of whether there are other order by disorder mechanisms that generalize the case considered here and whether these would produce different decision making among the 120° manifold of states. The answer is likely yes: one could increase the spin representation of the fermion degree of freedom from spin $1/2$ to another spin S as in the study of Ref. [17] who also consider the kagome lattice. This would enable the order by disorder effect to occur at other fillings than $1/2$ with potentially different Berry flux desires. Spin representation could therefore introduce a hierarchy of order by disorder mechanisms each possibly selecting a different state. Another generalization is the case where the electron hops over a spin and feels its presence via a term

$$H_{\text{spin hop}} = -t_{\text{spin}} \sum_{\langle ij\rangle} c^\dagger_{i\sigma} \vec{S}_{ij} \cdot \tau_{\sigma\sigma'} c_{i\sigma'} + \text{H.c.} = \sum_{\langle ij\rangle} c^\dagger_i \mathbf{U}_{ij} c_j. \tag{17}$$

This term involves a spatial SU(2) gauge field $\mathbf{U}_{ij}$ and so should select states different from the temporal SU(2) gauge field $\mathbf{A}_{0i}$ of Eq. (12) (possibly favoring spin chirality). So, order by disorder via fermion hopping with Berry flux could provide a rich set of decision making capabilities on the kagome 120° manifold and other such manifolds common in highly frustrated magnetism.

ACKNOWLEDGMENTS

We thank the late Christopher Henley for guidance during the early stages of this research. We also thank Shivam Ghosh for useful discussions.

[1] J. Villain, R. Bidaux, J.-P. Carton, and R. Conte, J. Phys. **41**, 1263 (1980).
[2] J. T. Chalker, in *Introduction to Frustrated Magnetism*, edited by C. Lacroix, P. Mendels, and F. Mila (Springer, Berlin, Heidelberg, 2011), pp. 3–22.
[3] M. Mitchell, *Complexity: A Guided Tour* (Oxford University Press, Oxford, UK, 2009).
[4] P. Chandra and B. Doucot, Phys. Rev. B **38**, 9335 (1988).
[5] C. L. Henley, Phys. Rev. Lett. **62**, 2056 (1989).
[6] A. L. Chernyshev and M. E. Zhitomirsky, Phys. Rev. B **92**, 144415 (2015).
[7] J. T. Chalker, P. C. W. Holdsworth, and E. F. Shender, Phys. Rev. Lett. **68**, 855 (1992).
[8] A. Chubukov, J. Appl. Phys. **73**, 5639 (1993).
[9] C. Henley and E. Chan, J. Magn. Magn. Mater. **140–144**, 1693 (1995).
[10] C. L. Henley, Phys. Rev. Lett. **96**, 047201 (2006).
[11] U. Hizi and C. L. Henley, Phys. Rev. B **80**, 014407 (2009).
[12] S. Ghosh, P. O'Brien, C. L. Henley, and M. J. Lawler, arXiv:1407.5354.
[13] R. Ozawa, S. Hayami, K. Barros, G.-W. Chern, Y. Motome, and C. D. Batista, J. Phys. Soc. Jpn. **85**, 103703 (2016).
[14] K. Pradhan and P. Majumdar, Europhys. Lett. **85**, 37007 (2009).
[15] H. Ishizuka and Y. Motome, Phys. Rev. Lett. **109**, 237207 (2012).
[16] Y. Akagi and Y. Motome, J. Korean Phys. Soc. **63**, 405 (2013).
[17] M. Udagawa, H. Ishizuka, and Y. Motome, JPS Conf. Proc. **014009**, 6 (2013).
[18] K. Barros, J. W. F. Venderbos, G.-W. Chern, and C. D. Batista, Phys. Rev. B **90**, 245119 (2014).
[19] L. Messio, B. Bernu, and C. Lhuillier, Phys. Rev. Lett. **108**, 207204 (2012).
[20] J. Ye, Y. B. Kim, A. J. Millis, B. I. Shraiman, P. Majumdar, and Z. Tešanović, Phys. Rev. Lett. **83**, 3737 (1999).
[21] K. Ohgushi, S. Murakami, and N. Nagaosa, Phys. Rev. B **62**, R6065(R) (2000).
[22] N. Nagaosa, J. Phys. Soc. Jpn. **75**, 042001 (2006).
[23] I. Martin and C. D. Batista, Phys. Rev. Lett. **101**, 156402 (2008).
[24] L. N. Bulaevskii, C. D. Batista, M. V. Mostovoy, and D. I. Khomskii, Phys. Rev. B **78**, 024402 (2008).
[25] S.-S. Gong, W. Zhu, L. Balents, and D. N. Sheng, Phys. Rev. B **91**, 075112 (2015).
[26] E. F. Shender, V. B. Cherepanov, P. C. W. Holdsworth, and A. J. Berlinsky, Phys. Rev. Lett. **70**, 3812 (1993)
[27] P. Chandra, P. Coleman, and I. Ritchey, J. Phys. I **3**, 591 (1993).
[28] Y. Makeenko, *Methods of Contemporary Gauge Theory* (Cambridge University Press, Cambridge, UK, 2002).
[29] T. Fukui, Y. Hatsugai, and H. Suzuki, J. Phys. Soc. Jpn. **74**, 1674 (2005).